Sahoo, Subhadyuti ; Jastrzebski, Rafał P.; Kepsu, Daria; Zenger, Kai; Jaatinen, Pekko; Pyrhonen, Olli

Modelling and Model-Based Control of A Bearingless 100 kW Electric Motor for High-Speed Applications

Published in:
Proceedings of the 2018 20th European Conference on Power Electronics and Applications (EPE'18 ECCE Europe)

Published: 01/09/2018

Document Version
Peer-reviewed accepted author manuscript, also known as Final accepted manuscript or Post-print

Please cite the original version:
Sahoo, S., Jastrzebski, R. P., Kepsu, D., Zenger, K., Jaatinen, P., & Pyrhonen, O. (2018). Modelling and Model-Based Control of A Bearingless 100 kW Electric Motor for High-Speed Applications. In *Proceedings of the 2018 20th European Conference on Power Electronics and Applications (EPE'18 ECCE Europe)* (European Conference on Power Electronics and Applications). IEEE. https://ieeexplore.ieee.org/document/8515453

Modelling & Model-Based Control of A Bearingless 100 kW Electric Motor for High-Speed Applications

Subhadyuti Sahoo[‡§], Rafal Jastrzebski[§], Daria Kepsu[§], Kai Zenger[‡], Pekko Jaatinen[§], Olli Pyrhönen[§]
[‡]AALTO UNIVERSITY, [§]LAPPEENRANTA UNIVERSITY OF TECHNOLOGY
[‡]Maarintie 8, 02150 / [§]Skinnarilankatu 34, 53850
[‡]Espoo, Finland / [§]Lappeenranta, Finland
Email: [‡]{firstname.lastname}@aalto.fi, [§]{firstname.lastname}@lut.fi
[‡]URL: http://www.aalto.fi/en/, [§]URL: https://www.lut.fi/web/en

ACKNOWLEDGEMENTS

The work has been co-funded by Academy of Finland No. 270012, No. 304071 and 304784, as well as by Business Finland Dnro 1170/31/2016.

KEYWORDS

≪Permanent magnet motor≫, ≪Magnetic bearings≫, ≪Modelling≫, ≪Optimal control≫, ≪Digital control≫, ≪Industrial application≫

ABSTRACT

This paper presents model-based control (MBC) analyses of a bearingless interior permanent magnet motor (IPMM). The motor is capable of producing 100 kW power for use in high-speed applications in industries. The maximum speed of the motor is 22000 rpm. Motor's initial parameters are obtained through Finite Element Method (FEM) analyses. State-space models, controller and observer matrices are built based on the optimal, operating points obtained from FEM analyses. Thereafter, the rotor's magnetic levitation characteristics are analyzed through digital control strategies. Performances of the controlled system are recorded and subsequently discussed.

I. INTRODUCTION

The use of magnetically levitated motors for various applications, especially in pumps, have seen an unprecedented rise in the last few years. Consequent-pole permanent magnet motors can assist in industrial canned pump applications because of wide magnetic air-gaps with respect to its rotor radius[1][2][3][4]. Reluctance motors with bearingless technology can find applications in high temperature or intense temperature variation operations due to its advantages like fail safe, robustness and low cost[1][5][6][7]. Bearingless induction motors have the advantage that they can be levitated with lesser voltage-ampere requirements[1][8]. They usually have additional windings in the stator. In 2002 centrifugal pumps were designed without bearings[9]. These were later used in medical applications, where flow rates of upto 18 liters could be easily achieved. Axial-type self-bearing motors were first developed in 2005 to function as artificial blood pump in order to pump blood during cardiopulmonary by-pass [10][11]. 300 W permanent magnet synchronous motor was designed in 2012 for bioreactor mixing[12]. Bearingless motors with 2500 W and 50 Nm torque production capability were designed in 2012 for pharmaceutical mixing applications[13]. Such motors could also be used in wastewater treatment plants[14].
This paper presents the modelling of forces of a twin unit 3-phase 100 kW interior permanent magnet motor (IPMM) and subsequent control of those forces for optimal levitation purposes. The rotational

speed is limited by the interior permanent magnet (IPM) rotor strength to centrifugal forces. For the control part, model-based control techniques are implemented. Model-based control techniques have been investigated before, but not for any bearingless motor with 5-degrees-of-freedom[15][16][17]. The FEM analyses are previously conducted for this motor prototype[18]. The standard motor design parameters, for our work, are derived by analytical methods from [18], [19], [20] and [21]. The design allows adding of suspension windings without significantly oversizing the overall motor design. The axial suspension is realized by a thrust bearing located between two motor-radial bearing units. The parameters of a single bearingless motor unit having 50 kW output are listed in [18]. Two such units produce 100 kW power. One unit has two sets of 3-phase windings – one for rotor suspension force generation and the other for motor operation[15]. Calculations and subsequent modelling of various forces acting upon the rotor are shown in Chapter II. Chapter III deals with the dissection of these forces into state-space models for model-based control of rotor's radial position. Proposed control scheme's analyses are discussed in Chapter IV. Simulation results are discussed in Chapter V.

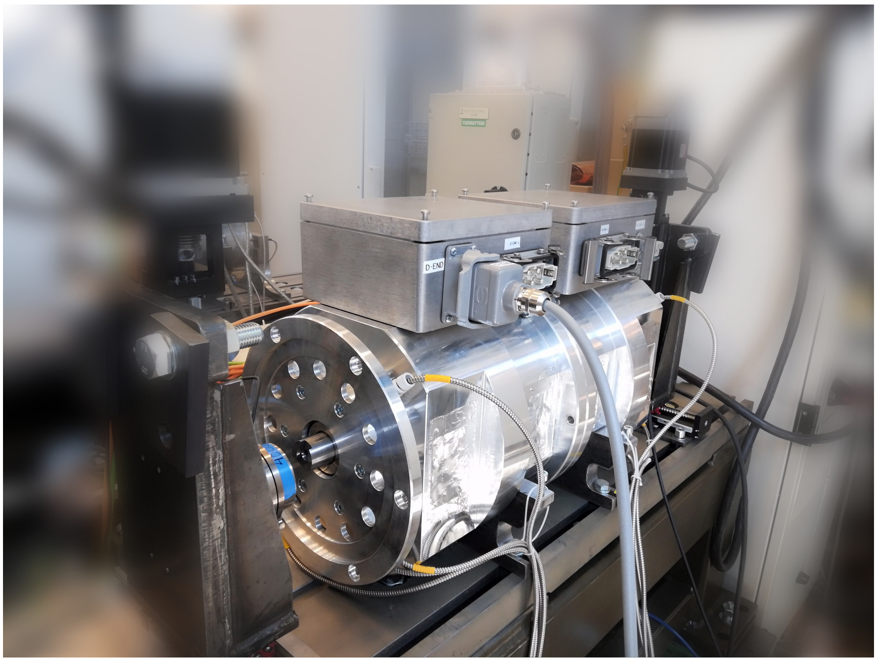

Fig. 1: 100 kW machine

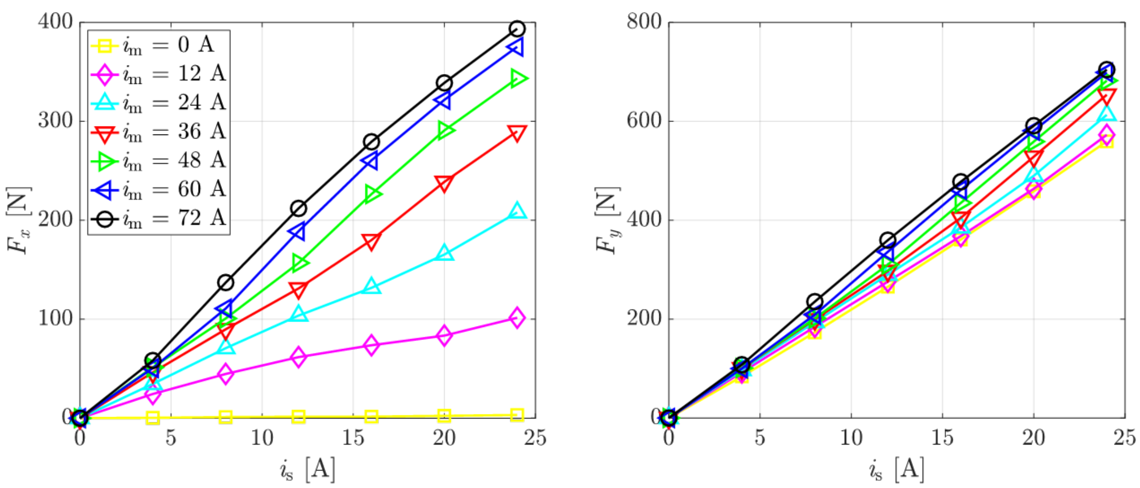

Fig. 2: Forces upon rotor from *x*- and *y*-directions as a function of suspension and motor currents

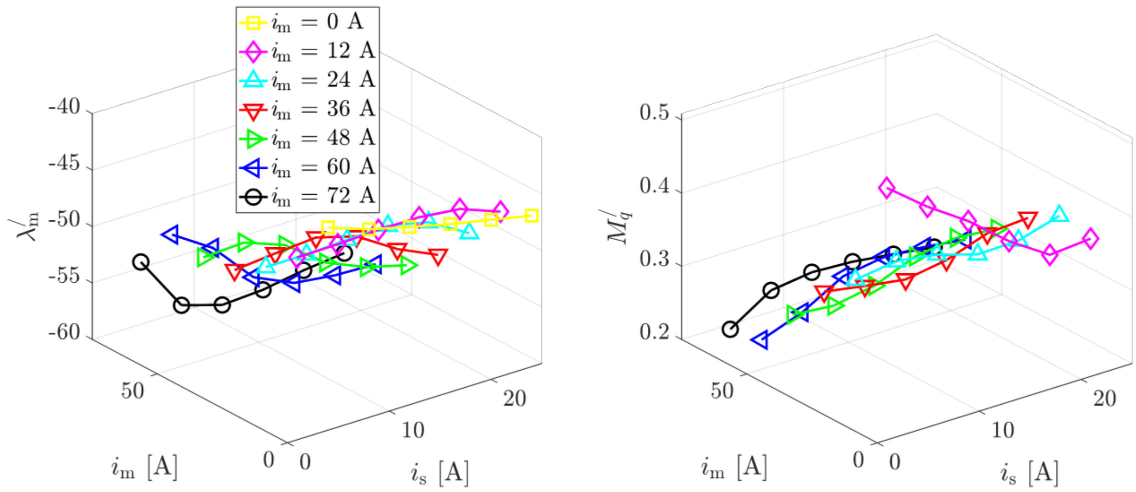

Fig. 3: Variation of $\lambda_m^{\prime}$ and $M_q^{\prime}$ as a function of suspension and motor currents

II. Modelling of Forces

Fig. 2 presents the radial forces acting on the rotor from x- and y-directions, with respect to the suspension currents and motor current values. These forces are evaluated from the mean force amplitudes and mean force angles in [18].

The suspension forces (F_x and F_y) are obtained from partial derivative of the stored magnetic energy (W_m) with respect to rotor's radial displacements (x and y). Eq. 1 shows the relation. $\lambda_m^{\prime}$ corresponds to current stiffness in active magnetic bearings (AMBs), $M_d^{\prime}$ is the suspension force constant in d-axis of the motor, i_{md} is the motor current in d-axis, $M_q^{\prime}$ is the suspension force constant in q-axis, i_{mq} is the motor current in q-axis, i_{sd} is the suspension current in d-axis and i_{sq} is the suspension current in q-axis[21].

$$\begin{bmatrix} F_x \\ F_y \end{bmatrix} = \begin{bmatrix} \frac{\partial W_m}{\partial x} \\ \frac{\partial W_m}{\partial y} \end{bmatrix} = \begin{bmatrix} \frac{1}{2}\lambda_m^{\prime} + M_d^{\prime} i_{md} & M_q^{\prime} i_{mq} \\ M_q^{\prime} i_{mq} & -\frac{1}{2}\lambda_m^{\prime} - M_d^{\prime} i_{md} \end{bmatrix} \begin{bmatrix} i_{sd} \\ i_{sq} \end{bmatrix} \tag{1}$$

Motor current i_{md} is assumed to be zero for suspension force control. Together with the position stiffness and gravitational force –

$$\begin{bmatrix} F_x \\ F_y \end{bmatrix} = \begin{bmatrix} (k_{x1} + k_{x2} i_{mq})x \\ (k_{x1} + k_{x2} i_{mq})y \end{bmatrix} + \begin{bmatrix} 0.5\lambda_m^{\prime} & M_q^{\prime} i_{mq} \\ M_q^{\prime} i_{mq} & -0.5\lambda_m^{\prime} \end{bmatrix} \begin{bmatrix} i_{sd} \\ i_{sq} \end{bmatrix} + \begin{bmatrix} 0 \\ -m_r g_a \end{bmatrix} \tag{2}$$

– where, k_{x1} and k_{x2} are the two position stiffnesses respectively, m_r is the point mass of the rotor and g_a is the acceleration due to gravity. The values for k_{x1} and k_{x2} are also obtained through FEM analyses[18]. The air-gap (a_g) for the motor is 0.9 mm. The $\lambda_m^{\prime}$ and $M_q^{\prime}$ values around the nominal operating point are chosen based on how they are varying with change in i_{mq}, i_{sd} and i_{sq} values. Fig. 3 describes the relationship of $\lambda_m^{\prime}$ and $M_q^{\prime}$ with the same increasing values of both the suspension and motor currents. It can be observed from Fig. 3 that, $\lambda_m^{\prime}$ and $M_q^{\prime}$ remain almost constant around i_s = 12 A. Hence, median of all the values of $\lambda_m^{\prime}$ and $M_q^{\prime}$ around this particular i_s value are calculated and those calculated values are chosen for nominal operation of the motor. The nominal i_m^{rms} was finalized to be 42.43 A, based on the values of $\lambda_m^{\prime}$ and $M_q^{\prime}$. Nominal values, used for building the controller and observer gain matrices, in rotor reference frame are presented in Table I.

Table I: Nominal Values

Quantities	Nominal Values	Ranges
$i_{\mathrm{m}q}^{rms}$	42.43 (A)	-50.91 (A) $\leqslant i_{\mathrm{m}q}^{rms} \leqslant$ 50.91 (A)
$i_{\mathrm{s}d}^{rms}$	8.49 (A)	-16.97 (A) $\leqslant i_{\mathrm{s}d}^{rms} \leqslant$ 16.97 (A)
$i_{\mathrm{s}q}^{rms}$	8.49 (A)	-16.97 (A) $\leqslant i_{\mathrm{s}q}^{rms} \leqslant$ 16.97 (A)
$\lambda_{\mathrm{m}}^{'}$	-56.85 (NA^{-1})	-59.95 (NA^{-1}) $\leqslant \lambda_{\mathrm{m}}^{'} \leqslant -50.00$ (NA^{-1})
$M_q^{'}$	0.26 (NA^{-2})	0.20 (NA^{-2}) $\leqslant M_q^{'} \leqslant$ 0.30 (NA^{-2})
k_{x1}	954450 (Nm^{-1})	Not Applicable
k_{x2}	8480.6 (NA^{-1}m^{-1})	Not Applicable
m_r	8 (kg)	Not Applicable
g_a	9.81 (ms^{-2})	Not Applicable
a_g	0.9 (mm)	Not Applicable

III. MODEL-BASED CONTROL

A. State-Space Models

For the model-based control of rotor's radial positions a near-accurate state-space model needs to be formed from the modelled forces. The velocities and positions, in both x- and y-directions, are taken as states for our system. The outputs are certainly the rotor's radial positions in x- and y-directions.

Fig. 4 shows the desired control structure for the motor system. The Controller stabilizes the non-linear system. The Estimator accounts for the unmeasured state(s), if any. The Integrator cancels out the steady-state errors.

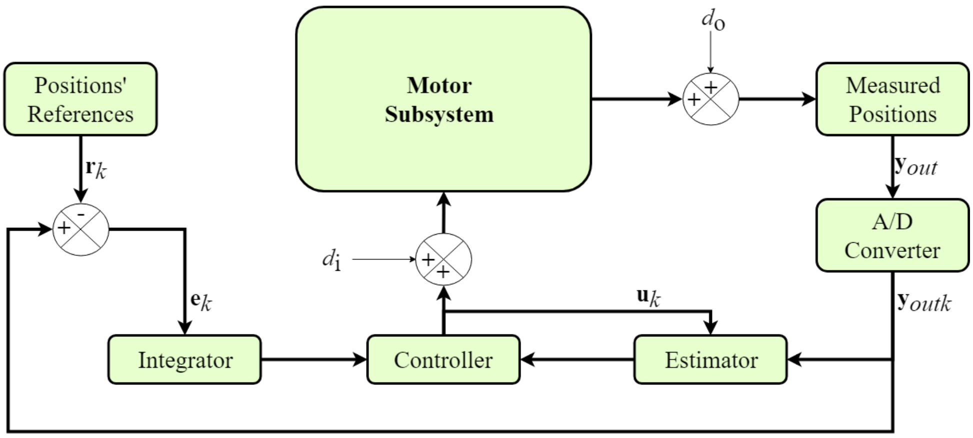

Fig. 4: Control Structure in Rotating Reference Frame

The $\mathbf{x}_{sp}$ matrix, in Eq. 3 and Eq. 4, constitutes the states of the system, $\mathbf{u}$ contains all the inputs, $\mathbf{y}_{out}$ contains the outputs; $\mathbf{A}$, $\mathbf{B}$, $\mathbf{C}$ and $\mathbf{D}$ are the state-space matrices; $\mathbf{x}_{nlsp}$, $\mathbf{u}_{nlsp}$, $\mathbf{u}_{grav}$, $\mathbf{A}_{nl}$ and $\mathbf{B}_{nl}$ are those matrices which contribute to non-linearity of the system. $\ddot{x}$, $\ddot{y}$ are the accelerations and $\dot{x}$, $\dot{y}$ are the velocities in x- and y-directions respectively. $i_{\mathrm{m}q}$ is needed to be kept separated from the linear portions, so that the steady-state performances of the levitated rotor can be free from the influence of the q-axis motor current. The decoupling of the inputs was necessary in order to nullify, as much as possible, the diagonal effect. Diagonal effect can be defined here as the change in y-axis rotor position due to changes in d-axis suspension current. The effect is also valid for relationship between x-axis rotor position and q-axis suspension current.

B. Control Law

The control law, for the system, is written as $\mathbf{u}_k = -\mathbf{K_I}\mathbf{x}_{\mathbf{I}(k)} - \mathbf{K}\hat{\mathbf{x}}_k$, where $\mathbf{u}_k$ is the discrete equivalent of $\mathbf{u}$, $\mathbf{K_I}$ is the integral gain matrix, $\mathbf{x}_{\mathbf{I}(k)}$ contains the error-integrated states, $\mathbf{K}$ is the controller gain matrix, $\hat{\mathbf{x}}_k$ contains the discrete estimated states, while $\mathbf{x}_k$ is the discrete equivalent of $\mathbf{x}_{sp}$. The error is considered as $\mathbf{e}_k = \mathbf{y}_{outk} - \mathbf{r}_k$, where $\mathbf{r}_k$ is the desired rotor's radial position, i.e., $[0\ 0]^{\mathrm{T}}$, also called reference matrix, and $\mathbf{y}_{outk}$ is the discrete equivalent of $\mathbf{y}_{out}$. This error vanishes in presence of an integrator. Such integration of steady-state errors form the $\mathbf{x}_{\mathbf{I}(k)}$ vector. The closed-loop augmented state-space equations, after incorporating the control law, is given in Eq. 5 where $\mathbf{F}$ and $\mathbf{G}$ are discrete equivalents of $\mathbf{A}$ and $\mathbf{B}$ respectively, $\mathbf{F}_{aug}$ and $\mathbf{G}_{aug}$ are the augmented discrete state-space matrices, $\mathbf{L}$ is the estimator gain matrix, $\mathbf{I}$ is an identity matrix and $\mathbf{O}$ is a zero matrix, the last two being of proper orders. The controller and estimator gain matrices are obtained from discrete linear quadratic regulator which minimizes the quadratic cost function given by $J = \sum_{k=1}^{\infty} (\mathbf{x}_k^{\mathrm{T}}\mathbf{Q}\mathbf{x}_k + \mathbf{u}_k^{\mathrm{T}}\mathbf{R}\mathbf{u}_k)$, where $\mathbf{Q}$ and $\mathbf{R}$ are weight matrices for states and inputs, respectively.

$$\underbrace{\begin{bmatrix}\ddot{x}\\ \dot{x}\\ \ddot{y}\\ \dot{y}\end{bmatrix}}_{\dot{\mathbf{x}}_{sp}} = \underbrace{\begin{bmatrix}0 & \frac{k_{x1}}{m_r} & 0 & 0\\ 1 & 0 & 0 & 0\\ 0 & 0 & 0 & \frac{k_{x1}}{m_r}\\ 0 & 0 & 1 & 0\end{bmatrix}}_{\mathbf{A}} \underbrace{\begin{bmatrix}\dot{x}\\ x\\ \dot{y}\\ y\end{bmatrix}}_{\mathbf{x}_{sp}} + \underbrace{\begin{bmatrix}\frac{0.5\lambda_{\mathrm{m}}'}{m_r} & 0\\ 0 & 0\\ 0 & -\frac{0.5\lambda_{\mathrm{m}}'}{m_r}\\ 0 & 0\end{bmatrix}}_{\mathbf{B}} \underbrace{\begin{bmatrix}i_{sd}\\ i_{sq}\end{bmatrix}}_{\mathbf{u}} + \underbrace{\begin{bmatrix}\frac{k_{x2}}{m_r} & 0\\ 0 & 0\\ 0 & \frac{k_{x2}}{m_r}\\ 0 & 0\end{bmatrix}}_{\mathbf{A}_{nl}} \underbrace{\begin{bmatrix}xi_{\mathrm{m}q}\\ yi_{\mathrm{m}q}\end{bmatrix}}_{\mathbf{x}_{nlsp}} +$$

$$\underbrace{\begin{bmatrix}0 & \frac{M_q'}{m_r}\\ 0 & 0\\ \frac{M_q'}{m_r} & 0\\ 0 & 0\end{bmatrix}}_{\mathbf{B}_{nl}} \underbrace{\begin{bmatrix}i_{sd}i_{\mathrm{m}q}\\ i_{sq}i_{\mathrm{m}q}\end{bmatrix}}_{\mathbf{u}_{nlsp}} + \underbrace{\begin{bmatrix}0\\ 0\\ -g_a\\ 0\end{bmatrix}}_{\mathbf{u}_{grav}} \tag{3}$$

$$\underbrace{\begin{bmatrix}x\\ y\end{bmatrix}}_{\mathbf{y}_{out}} = \underbrace{\begin{bmatrix}0 & 1 & 0 & 0\\ 0 & 0 & 0 & 1\end{bmatrix}}_{\mathbf{C}} \underbrace{\begin{bmatrix}\dot{x}\\ x\\ \dot{y}\\ y\end{bmatrix}}_{\mathbf{x}_{sp}} + \underbrace{\begin{bmatrix}0 & 0\\ 0 & 0\end{bmatrix}}_{\mathbf{D}} \underbrace{\begin{bmatrix}i_{sd}\\ i_{sq}\end{bmatrix}}_{\mathbf{u}} = \mathbf{C}\mathbf{x}_{sp} \tag{4}$$

$$\underbrace{\begin{bmatrix}\mathbf{x}_{\mathbf{I}(k+1)}\\ \mathbf{x}_{k+1}\\ \hat{\mathbf{x}}_{k+1}\end{bmatrix}}_{\mathbf{x}_{aug(k+1)}} = \underbrace{\begin{bmatrix}\mathbf{I} & \mathbf{C} & \mathbf{O}\\ -\mathbf{G}\mathbf{K}_{\mathbf{I}} & \mathbf{F} & -\mathbf{G}\mathbf{K}\\ -\mathbf{G}\mathbf{K}_{\mathbf{I}} & \mathbf{L}\mathbf{C} & (\mathbf{F}-\mathbf{G}\mathbf{K}-\mathbf{L}\mathbf{C})\end{bmatrix}}_{\mathbf{F}_{aug}} \underbrace{\begin{bmatrix}\mathbf{x}_{\mathbf{I}(k)}\\ \mathbf{x}_{k}\\ \hat{\mathbf{x}}_{k}\end{bmatrix}}_{\mathbf{x}_{aug(k)}} + \underbrace{\begin{bmatrix}-\mathbf{I}\\ \mathbf{O}\\ \mathbf{O}\end{bmatrix}}_{\mathbf{G}_{aug}} \mathbf{r}_k \tag{5}$$

IV. CONTROL ANALYSES

Fig. 5 presents the pole-zero map and step response analyses of the controlled system. The poles of the controlled plant are well within the unit circle (in discretized form), which indicates that the controlled plant is asymptotically stable. The step responses show that output 1 primarily changes with change in input 1 and similar is the case with output 2 and input 2. However, diagonal effects − that is, change in output 2 with change in input 1 and change in output 1 with change in input 2 − are present, but they settle down quickly due to controller action, indicating controllable diagonal effects.

Fig. 6 shows the magnitudes for reference-to-error ($\mathbf{r}_k$-$\mathbf{e}_k$) sensitivity and output-disturbance-to-output (d_{o}-$\mathbf{y}_{out}$) sensitivity. The maximum absolute magnitude for $\mathbf{r}_k$-$\mathbf{e}_k$ sensitivity is 1.19. The maximum absolute magnitude for d_{o}-$\mathbf{y}_{out}$ sensitivity is 1.46. It is later found through simulations that step input disturbances can be controlled if they are within 47% of maximum suspension current and step output disturbances can be controlled if they are within 55% of the nominal air-gap.

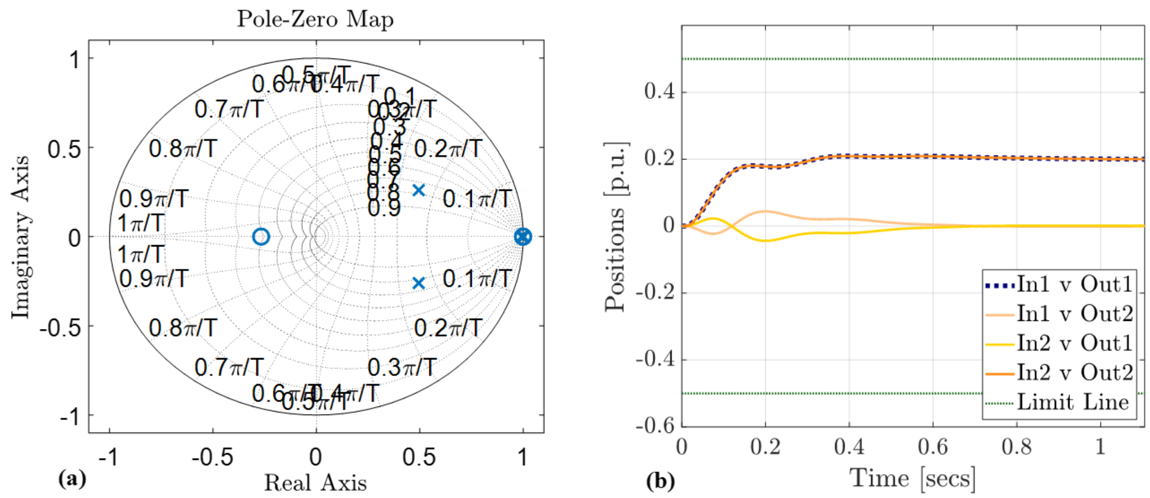

Fig. 5: (a) Pole-Zero Map, (b) Step Responses of the controlled system

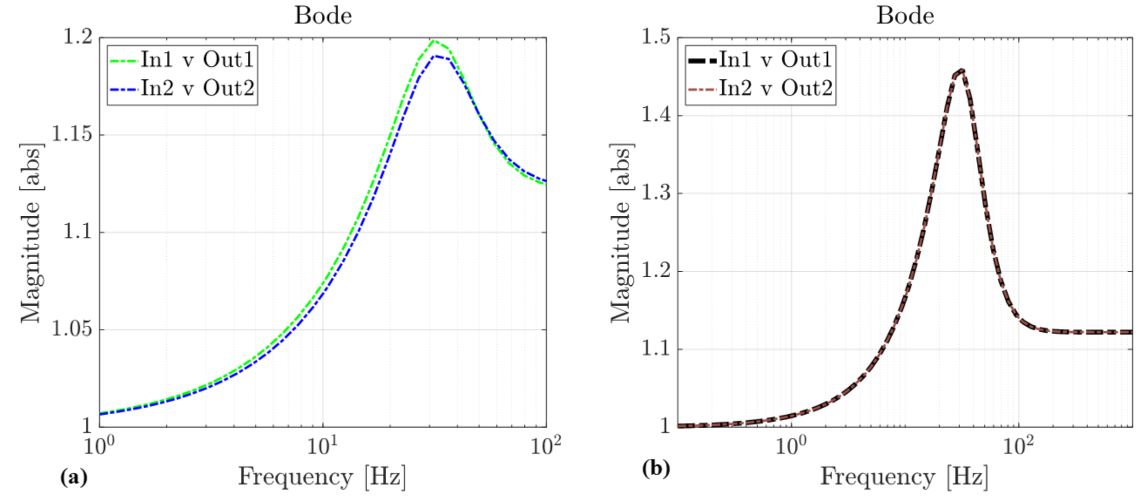

Fig. 6: (a) Reference-to-Error Sensitivity, (b) Output-Disturbance-to-Output Sensitivity

V. Simulation Results

A. Lift-Up

The rotor needs to be lifted up before any operation can be started. Fig. 7 shows the rotor lift-up dynamics. Since the maximum allowable suspension current is 24 A, there are some oscillations in suspension currents towards the beginning which also lead to similar oscillations in the rotor positions. However, those position oscillations are well within the allowable limits, which are defined here as nearly half the air-gap in per-unit (p.u.) quantities. There are also oscillations in the forces along both the x- and y-axes, but with the stabilization of the controlled suspension currents the forces also stabilize.

B. Step Responses and Motor Current

Fig. 8 presents the step responses of rotor positions, the corresponding control efforts in suspension currents and the forces' waveforms after steady-state conditions have been reached. The q-axis motor current is started, but after the step responses have died down. The rotor positions do not show any appreciable changes with the starting of the q-axis motor current. Performances of the estimators are satisfactory for the steady-state conditions. The errors in estimator are, however, on the higher side when step changes are made in the rotor positions' reference signals.

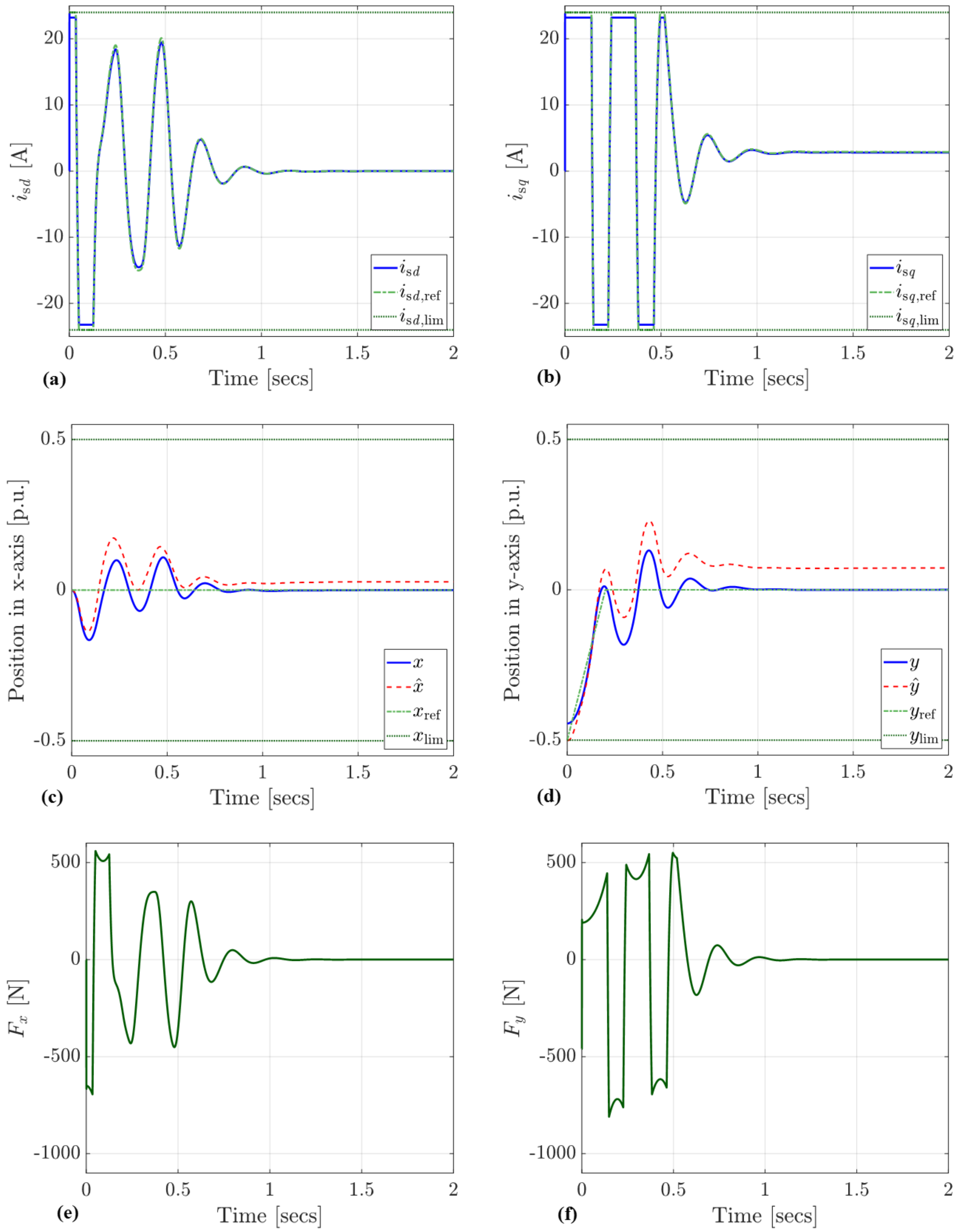

Fig. 7: Rotor Lift-Up Dynamics – (a) d-axis suspension current waveform, (b) q-axis suspension current waveform, (c) x-axis rotor position responses, (d) y-axis rotor position responses, (e) Suspension force waveform along x-axis, (f) Suspension force waveform along y-axis

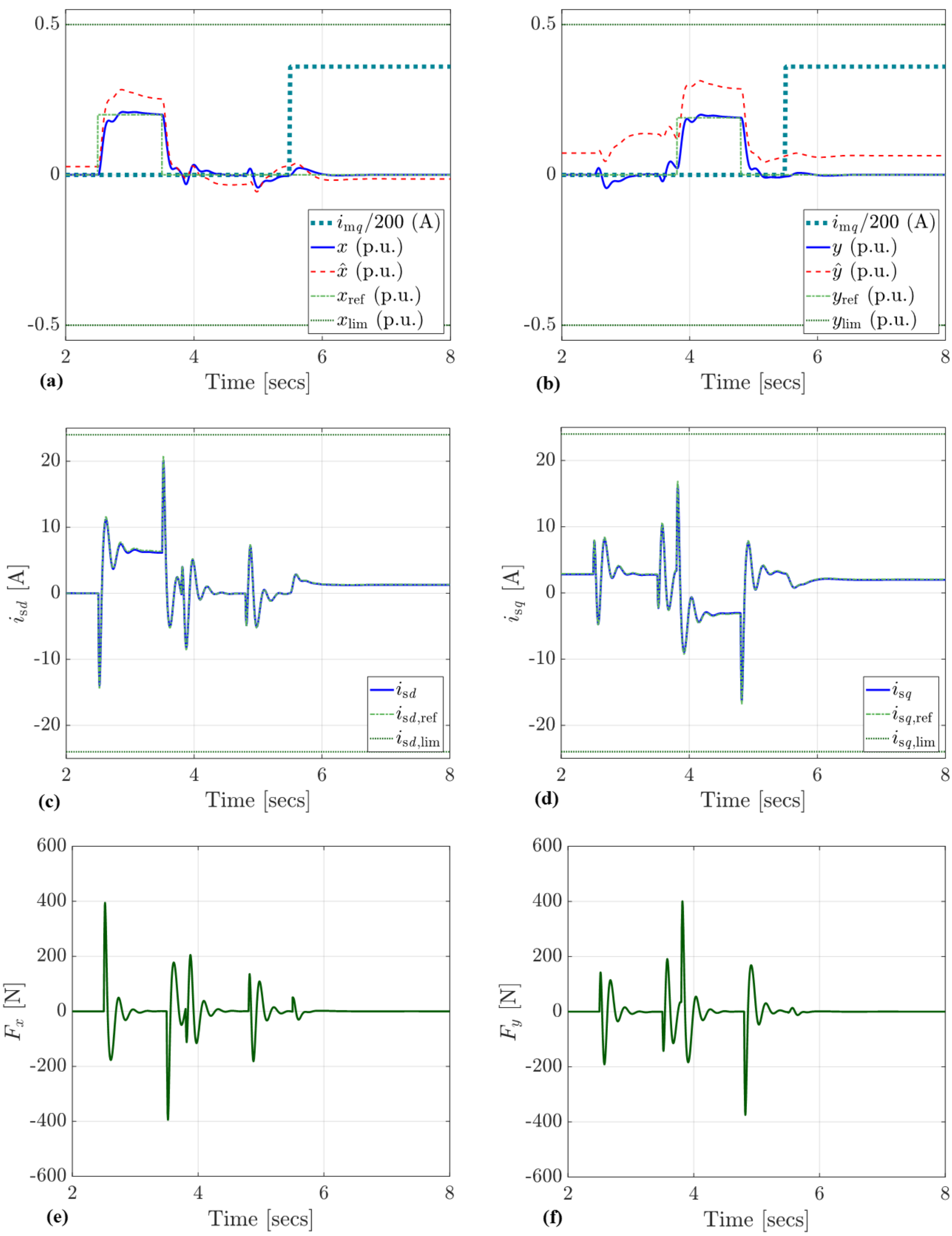

Fig. 8: Step Change & Motor Current Dynamics – (a) x-axis rotor position responses, (b) y-axis rotor position responses, (c) d-axis suspension current waveform, (d) q-axis suspension current waveform, (e) Suspension force waveform along x-axis, (f) Suspension force waveform along y-axis

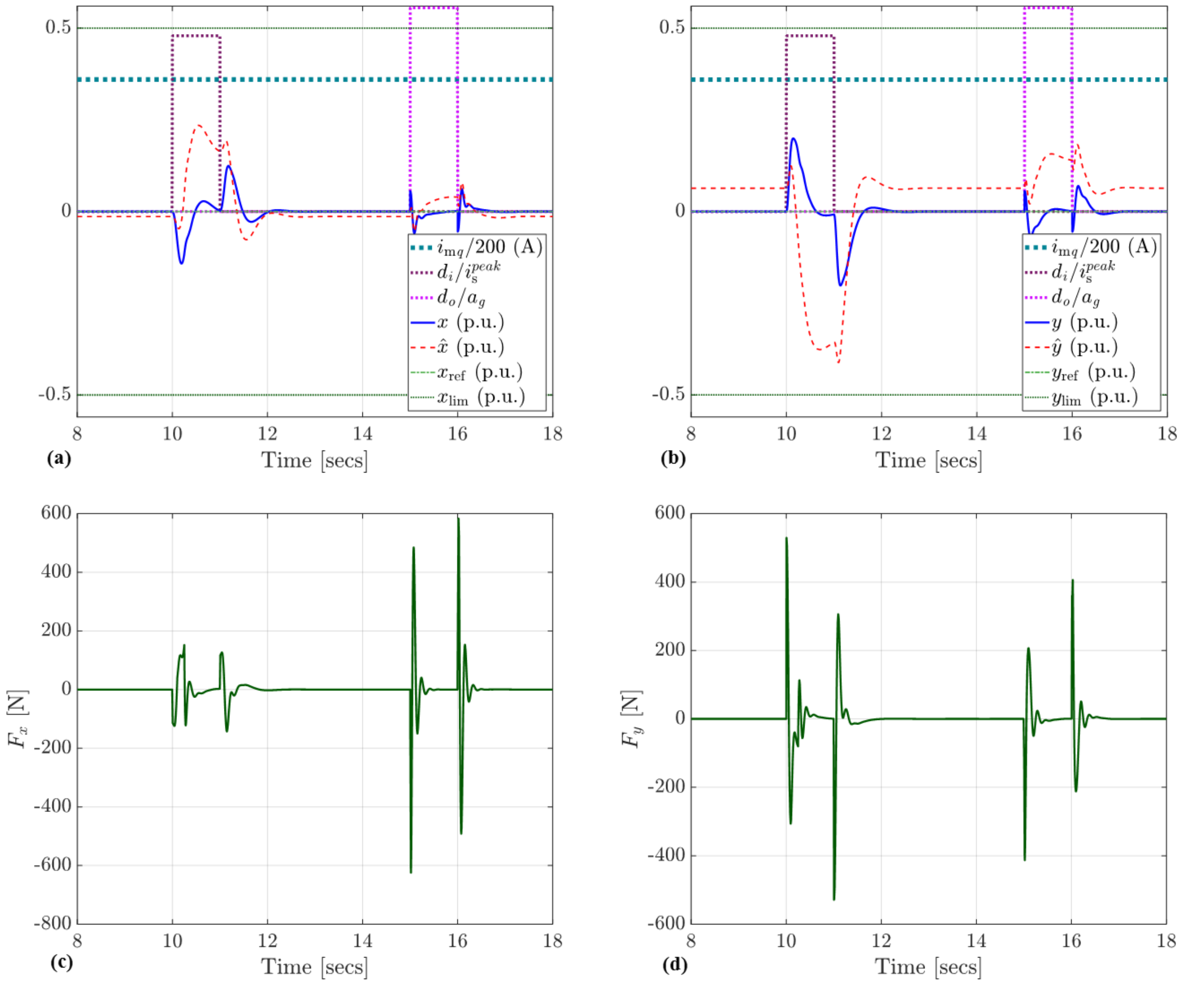

Fig. 9: Step Input & Output Disturbances Dynamics – (a) *x*-axis rotor positions responses, (b) *y*-axis rotor position responses, (c) Suspension force waveform along *x*-axis, (d) Suspension force waveform along *y*-axis

C. *Input and Output Disturbances*

Fig. 9 shows the responses of the rotor when there are step input and output disturbances. The step input disturbances are expressed in Fig. 9 as fractions of the maximum suspension currents. The step output disturbances are shown in Fig. 9 as a fraction of the air-gap. The controlled system is efficient in overcoming step input disturbances of the order of 47% of maximum suspension current. The controlled system is capable of rejecting step output disturbances of the order of 55% of the air-gap. There is an appreciable deviation of the rotor from the central position due to these disturbances. However, due to faster control action, the rotor is able to recover quite quickly and start following the central positions' references.

VI. Conclusions

In this paper, optimal and model-based control of levitation forces of a bearingless interior permanent magnet motor by means of its suspension currents are investigated. The motor is capable of producing 100 kW power for high-speed applications in industrial pumps and compressors, for instance. The levitation forces are initially broken down into state-space models, with velocities and positions in both *x*- and *y*-directions as states. A control law is formulated based on these models. Estimator and integrator are added.

The non-linear, coupled, time-continuous motor model is built in Simulink. It is fitted with discrete controller, estimator and integrator. Time-varying simulations are conducted on the entire model. Smooth lifting up of the rotor is considered in the beginning, which leads to controllable oscillations in the suspension currents. Similar oscillations also appear in the position responses because of the suspension currents' oscillations. However, these oscillations settle down faster and the rotor starts following its reference position unfailingly.
Hereafter, responses to step changes during steady state are recorded. The diagonal effects are present, but their amplitude are very small. Hence, the effects can be controlled. The motor current is started during the steady-state operation but it has little effect on the levitated rotor position.
Finally, responses to step input and output disturbances are investigated. The rotor gets shifted from the central position due to those disturbances. However, due to fast dynamics of the controller, rotor returns to the central position pretty quickly and starts following the reference signals. The motor system is successful in overcoming step input disturbances of the order of 47% of the maximum suspension current and step output disturbance of the order of 55% of the air-gap. The settling time after overcoming the disturbances was between 0.5 and 1 second.

References

[1] Bin L.: Survey of Bearingless Motor Technologies and Applications, IEEE ICMA 2015, pp. 1983-1988
[2] Asano Y., Mizuguchi A., Amada M., et al.: Development of A Four-Axis Actively Controlled Consequent-Pole-Type Bearingless Motor, IEEE Transactions on Industry Applications Vol. 45 no 4, pp 1378-1386
[3] Asama J., Nakamura R., Sugimoto H., et al.: Evaluation of Magnetic Suspension Performance in a Multi-Consequent-Pole Bearingless Motor, IEEE Transactions on Magnetics, Vol. 47 no 10, pp. 4262-4265
[4] Sugimoto H., Uemura Y., Chiba A., et al.: Design of homopolar consequent-pole bearingless motor with wide magnetic gap, IEEE Transactions on Magnetics, Vol. 49 no 5, pp. 2315-2318
[5] Gruber W., Briewasser W., Rothböck M., et al.: Bearingless slice motor concepts without permanent magnets in the rotor, IEEE ICIT 2013, pp. 259-265
[6] Rao J., Hijikata W., Shinshi T.: A bearingless motor utilizing a permanent magnet free structure for disposable centrifugal blood pumps, Journal of Advanced Mechanical Design, Systems, and Manufacturing, Vol. 9 no 3, pp. 1-16
[7] Recheis M., Schweighoffer B., Fulmek P., et al.: Selection of Magnetic Materials for Bearingless High-Speed Mobile Flywheel Energy Storage Systems, IEEE Transactions on Magnetics, Vol. 50 no 4
[8] Ito E., Chiba A., Fukao T.: A measurement of VA requirements in an induction type bearingless motor, Proceedings of the 4th International Symposium on Magnetic Suspension Technology
[9] Schöb R.: Centrifugal pump without bearings or seals, World Pumps, Vol. 2002 no 430, pp. 34-37
[10] Okada Y., Yamashiro N., Ohmori K., et al.: Mixed Flow Artificial Heart Pump With Axial Self-Bearing Motor, IEEE/ASME Transactions on Mechatronics, Vol. 10 no 6, pp. 658-665
[11] Yang S., Huang M.: Design and Implementation of a Magnetically Levitated Single-Axis Controlled Axial Blood Pump, IEEE Transactions on Industrial Electronics, Vol. 56 no 6, pp. 2213-2219
[12] Reichert T., Nussbaumer T., Kolar J. W.: Bearingless 300-W PMSM for Bioreactor Mixing, IEEE Transactions on Industrial Electronics, Vol. 59 no 3, pp. 1376-1388
[13] Warberger B., Kaelin R., Nussbaumer T., eta l.: 50-N.m/2500-W Bearingless motor for High-Purity Pharmaceutical Mixing, IEEE Transactions on Industrial Electronics, Vol. 59 no 5, pp. 2236-2247
[14] Severson E., Mohan N.: Bearingless motor System Design for Industrial Applications, IEEE IEMDC 2017
[15] Shafiq M., Akhtar S.: Inverse Model Based Adaptive Control of Magnetic Levitation System, IEEE ACC 2004, pp. 1414-1418
[16] Seban L., Sahoo N., Roy B.K.: Multiple Model based Predictive Control of Magnetic Levitation System, IEEE INDICON 2014
[17] Jiang Q., Liang D., Yan F., et al.: Force Sensor Model based on FEA for Electromagnetic Levitation System, Computing in Science & Engineering (Early Access), Vol. 20 no 1
[18] Jastrzebski R., Jaatinen P., Sugimoto H., et al.: Design of a bearingless 100 kW electric motor for high-speed applications, IEEE ICEMS 2015, pp. 2008-2014
[19] Pyrhönen, J., Jokinen T., Hrabovcová V., 2014: Design of Rotating Electrical Machines, 2nd edn, John Wiley & Sons: Chichester
[20] Hendershot, J.R., Miller, T.J.E., 2010: Design of Brushless Permanent-Magnet Machines, 2nd edn, Motor Design Books LLC: Venice
[21] Chiba A., Fukao T., Ichikawa O., et al., 2005: Magnetic Bearings and Bearingless Drives, 1st edn, Oxford: Newnes
[22] Franklin G.F., Powell J.D., Workman M.L., 1997: Digital Control of Dynamic Systems, 3rd edn, Addison Wesley Longman: Menlo Park
[23] Bryson A.E., Ho Y., 1975: Applied Optimal Control, 1st edn, Taylor & Francis Group, LLC: Abingdon
[24] Kwakernaak H., Sivan R., 1972: Linear Optimal Control Systems, 1st edn, John Wiley & Sons: Hoboken